

# Global approach for the reactions ${}^7\text{Be} + {}^{28}\text{Si}$ and ${}^7\text{Be} + {}^{208}\text{Pb}$ at near- and sub-barrier energies

O. Sgouros <sup>1</sup>, V. Soukeras <sup>1,2</sup>, K. Palli <sup>3,4</sup> and A. Pakou <sup>3,\*</sup>

<sup>1</sup>*INFN Laboratori Nazionali del Sud, via S. Sofia 62, 95125 Catania, Italy*

<sup>2</sup>*Dipartimento di Fisica e Astronomia “Ettore Majorana”, Università di Catania, via S. Sofia 64, 95125 Catania, Italy*

<sup>3</sup>*Department of Physics and HINP, The University of Ioannina, 45110 Ioannina, Greece*

<sup>4</sup>*Department of Chemistry, National and Kapodistrian University of Athens and HINP, 15771 Athens, Greece*



(Received 20 July 2022; accepted 17 October 2022; published 31 October 2022)

Elastic scattering, total reaction, and fusion cross section measurements for the radioactive  ${}^7\text{Be}$  nucleus on a light and a heavy target, are treated in a global approach at near and sub-barrier energies for probing the optical potential and describing fusion at low energies. Elastic scattering data of  ${}^7\text{Li}$  on the same target were analyzed under the same context to support this analysis. It is found that for low mass targets, dispersion relations are not adequate for describing the potential or the fusion. On the contrary this is possible for heavy targets, where the standard potential threshold anomaly and fusion enhancement is observed. The consequences of the above on fusion hindrance at deep sub-barrier energies is discussed.

DOI: [10.1103/PhysRevC.106.044612](https://doi.org/10.1103/PhysRevC.106.044612)

## I. INTRODUCTION

Fusion at below barrier energies, between other aspects, is an indispensable tool for understanding and probing the nuclear potential. At these energies, elastic scattering, the traditional observable for probing the optical potential, is dominated by Rutherford scattering, due to the strong interaction with the Coulomb potential, and therefore it is not adequate. At near and just below barrier energies the optical potential presents an anomaly, the potential threshold anomaly (TA). While for well bound nuclei this phenomenon related to coupling channel effects is well established, for weakly bound nuclei despite a long time effort, open questions persist. In this respect, global studies, including various observables between the fusion, are necessary to probe with significant liability the energy dependence of the optical potential and perhaps extrapolate it to deep sub-barrier energies. At these energies there is a lot of interest from the point of view of astrophysical problems. The threshold anomaly of the optical potential  $U(E) = V(E) + iW(E)$ , is understood as a rapid variation of the imaginary part which decreases as we approach the barrier, due to the Coulomb repulsion leading to the closure of various reaction channels [1–3]. This is connected with a rapid increase of the real part going from lower to higher energies and then a decrease, with the development of a bell shaped maximum at barrier. This maximum was later understood as necessary for describing the fusion enhancement at near and below barrier energies due to coupling channel effects, both aspects of the potential threshold anomaly and fusion enhancement, being the two views of the same coin [1]. In this respect it is customary to express the real part with a correction term  $\Delta V(E)$ ,  $V(E) = V_0(E) + \Delta V(E)$ , named the dynamic polarization potential (DPP). If the causality

principle is satisfied then it was suggested by Mahaux independently by Nagarajan, and reported in detail by Satchler in Ref. [1], that an appropriate mathematical tool to connect the two quantities,  $\Delta V(E)$  and  $W(E)$ , is a dispersion relation. We intend in this article, in a global approach, to probe the optical potential and simultaneously to investigate these aspects from the phenomenological point of view. The example case will be related with the radioactive nucleus  ${}^7\text{Be}$  on a light and heavy target,  ${}^{28}\text{Si}$  and  ${}^{208}\text{Pb}$ , respectively. Questions to be posed are: Does the dispersion relation break down (causality principle) for the connection of the imaginary and real parts of the optical potential for weakly bound nuclei like  ${}^7\text{Be}$ ? Can fusion be described by one Barrier Penetration Model (BPM) if explicitly we take into account the energy dependence of the optical potential? Could these calculations help for probing the phenomenon of fusion hindrance [4,5]? Are the theoretical coupling channel models, such as the continuum discretized coupled channel (CDCC), capable of describing both elastic scattering and fusion and therefore is excitation to continuum a strong player to such problems?

${}^7\text{Be}$  is an interesting weakly bound proton rich nucleus with an  ${}^4\text{He} + {}^3\text{He}$  cluster structure. Its breakup threshold is 1.59 MeV to be compared with 2.47 MeV for the mirror  ${}^7\text{Li}$ . We note that the breakup threshold for  ${}^6\text{Li}$  is 1.47 MeV and a debate exists in the literature about the resemblance of the behavior of  ${}^7\text{Be}$  to one or the other weakly bound lithium projectiles [6–9]. This issue will be also revisited here.

${}^7\text{Be}$ , except this interesting structure, attracts vivid attention in problems of astrophysics. It is well known and still not fully resolved that the cosmological lithium problem [10] with respect to the discrepancy between the measurement and the big bang nucleosynthesis (BBN) predicted abundance. In BBN, it is produced via  ${}^7\text{Be}$ , therefore the production [ ${}^3\text{He}(\alpha, \gamma){}^7\text{Be}$ ] and destruction [ ${}^7\text{Be}(n, \alpha){}^4\text{He}$  and  ${}^7\text{Be}(n, p){}^7\text{Li}$ ] of this nucleus is of vital importance [11–14]. And while the present research is not directly connected with such problems,

\*apakou@uoi.gr

every piece of information connected with the behavior of  ${}^7\text{Be}$  in reactions with various elements may disclose solutions to various problems. Important ingredients in such calculations (see, e.g., Ref. [14]) are the binding potentials like the ( ${}^4\text{He}$ - ${}^3\text{He}$ ) one, used also in, e.g., CDCC calculations for elastic scattering and the breakup of this nucleus. We will also touch this point by adopting this binding potential.

In what follows in Sec. II, we will present our phenomenological description of the potential through elastic scattering and fusion existing data for the system  ${}^7\text{Be} + {}^{28}\text{Si}$ . CDCC calculations will be also included. Relevant results for  ${}^7\text{Be} + {}^{208}\text{Pb}$  will be presented in Sec. III. The consequences of the above descriptions in connection with fusion hindrance for both systems will be presented in Sec. IV. Finally in Sec. V, we will discuss and compare our findings between the two targets, the light and the heavy one, while also making comparisons with the mirror  ${}^7\text{Li}$  weakly bound but stable projectile.

## II. THE SYSTEM ${}^7\text{Be} + {}^{28}\text{Si}$

### A. The phenomenological description

Previous elastic scattering data [9] were revisited for the needs of this work within the same formalism as before, adopting the double-folding model and the BDM3Y1 interaction [15]. For the stable target,  ${}^{28}\text{Si}$ , the nuclear matter density was adopted from electron scattering data [16], appropriately corrected to derive it. For the density of the radioactive  ${}^7\text{Be}$  nucleus, calculated values were used under a semiphenomenological expression reported in [16]. For the  ${}^7\text{Li}$  nucleus we used Hartree-Fock calculations obtained by Trache *et al.* [17]. These densities have been used in numerous articles before [9,18–21] with very good results. Calculations were not repeated with other densities, taking into account explicitly the cluster structure of projectiles since at these low energies, this structure cannot be effectively probed. The same potential as for the real part of the OMP was also adopted for the imaginary potential but with different normalization factor. The two normalization factors,  $N_R$  and  $N_I$  were best fitted to the data and the results related with the energy dependence of the potential, are shown in Fig. 1. Uncertainties were obtained through a sensitivity analysis of the elastic scattering data. It included a grid search, where at certain values of the real normalization factor of the BDM3Y1 interaction, below and above the best fitted value, the normalization factor of the imaginary potential is searched, such as to fit the data. The same was repeated with the normalization factor for the imaginary part of the potential. Previous results for  ${}^7\text{Li}$  and the same target, analyzed under the same theoretical context and reported in Ref. [18], are also presented for reasons of comparison. The trend for  ${}^7\text{Li}$  following the trend for  ${}^7\text{Be}$  clearly presents a drop for the imaginary part of the OM potential as we approach the barrier from higher to lower energies, and a flat trend for the real part. For  ${}^7\text{Be}$  the data points are few, determined with a large uncertainty, and an indication for a dispersive correction to the real part cannot be excluded [9]. To clarify this point other observables have

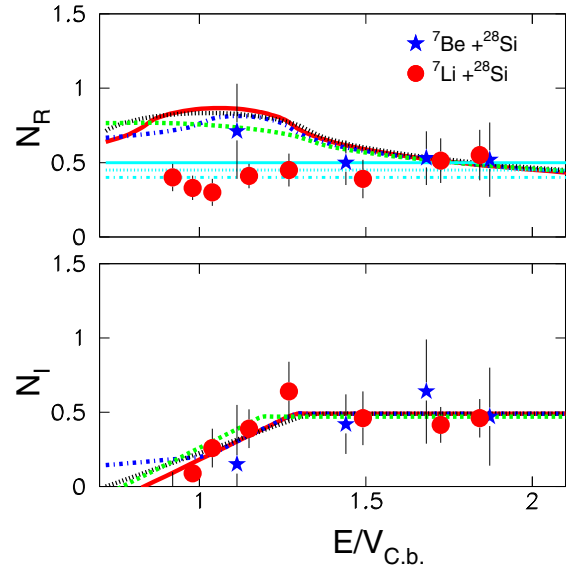


FIG. 1. Energy dependence of OMP for  ${}^7\text{Be} + {}^{28}\text{Si}$  in comparison with results for  ${}^7\text{Li} + {}^{28}\text{Si}$ . The lines for the imaginary part correspond to various trials for describing the potential with their relevant dispersion corrections on the real part of it. The flat cyan lines drawn in the real part will be discussed in the text. The Coulomb barrier was calculated according to Broglia [22].

to be taken into account [1,23]. In this respect, fusion data reported before [8] have been treated in this work in the same theoretical framework as the elastic scattering data, for validating the energy dependence of the potential. For that we attempted the description of the imaginary potential drawing several lines and into a two segment model [1], the dispersive correction was estimated for the real part and included in Fig. 1. An attempt was also made to describe the real part with flat lines between  $N_R = 0.4$  to  $0.5$ . Subsequently, BPM calculations were performed, adopting the ansatz suggested before [23–25], where the real part is taken from the elastic scattering results and the imaginary was expressed by a short-range Woods-Saxon form factor, such as to absorb all the flux penetrating the barrier, simulating the ingoing wave boundary conditions [24].

The total fusion cross sections were calculated with the code ECIS [25,26]. In Fig. 2, we present our BPM calculations according to the real potentials appearing through dispersion relations in Fig. 1. Also two calculations adopting the flat real potential, minimum, and maximum values ( $N_R = 0.4$  and  $N_R = 0.5$ ) were also performed and are shown in the same figure. We should note that the notation of the lines is the same in both Figs. 1 and 2 for easiness of the reader. It becomes evident that, taking into account any real potential extracted with the dispersive correction, the calculated total fusion cross sections are similar amongst themselves but strongly contrast those determined, taking into account the flat line (no dispersion correction). These phenomenological calculations are also compared in Fig. 3 with previously obtained data for  ${}^7\text{Be} + {}^{28}\text{Si}$  [8],  ${}^7\text{Be} + {}^{27}\text{Al}$  [27], and  ${}^7\text{Li} + {}^{28}\text{Si}$  [28–31], under

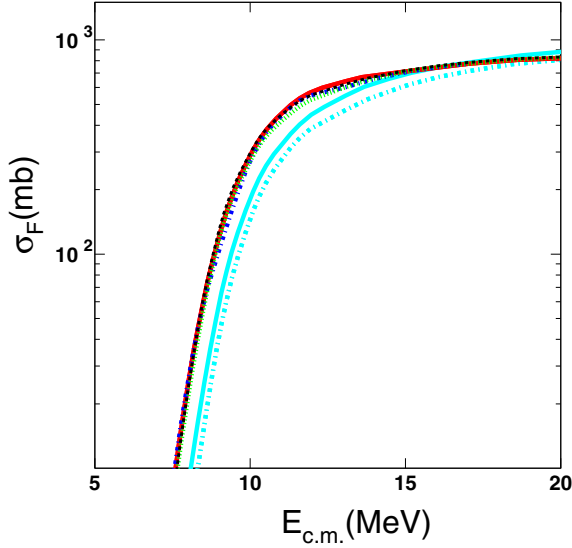


FIG. 2. Excitation fusion function of BPM calculations for  ${}^7\text{Be} + {}^{28}\text{Si}$  according to the potentials described in Fig. 1. The type of lines are the same as in Fig. 1.

a reduced form [32]

$$\sigma_F \rightarrow F(x) = \frac{2E_{c.m.}}{\hbar\omega R_B^2} \sigma_F \quad (1)$$

corresponding to an energy  $E_{c.m.}$  of the projectile reduced to the quantity  $x$  given by the equation

$$E_{c.m.} \rightarrow x = \frac{E_{c.m.} - V_B}{\hbar\omega} \quad (2)$$

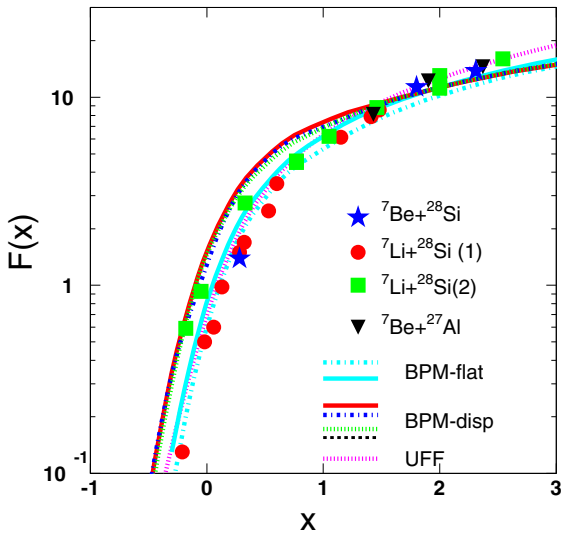


FIG. 3. Reduced total fusion excitation functions,  $F(x)$ , according to Ref. [32] and Eqs. (1) and (2), for  ${}^7\text{Be} + {}^{28}\text{Si}$ ,  ${}^7\text{Be} + {}^{27}\text{Al}$ ,  ${}^7\text{Li} + {}^{28}\text{Si}$  are compared amongst themselves. Data are from Refs. [8,27–31]. Lines are calculations in a BPM approach with real potentials as the ones appearing in Fig. 1.

TABLE I. Calculated total reaction cross sections for  ${}^7\text{Be} + {}^{28}\text{Si}$ , designated as flat1, flat2, and disp, are compared with phenomenological predictions [33], designated as pred. For flat1, the real potential is the one represented by a flat line at  $N_R = 0.5$ —see Fig. 1—and imaginary one designated in the same figure with the red solid line. For flat2, we adopt the same real potential as before but for the imaginary potential we adopt below  $E/V_{C.b.} = 1$  a constant line with  $N_I = 0.2$ . For the calculation under the name disp, we used the same imaginary as in flat1, but for the real we took into account the dispersive correction—red solid line in Fig. 1.

$E_{\text{lab}}$ (MeV)	$\sigma$ (mb)			
	flat1	flat2	disp	pred
10.4	35	54	64	56
11.6	158	162	216	170
13	356		417	347
17	817		827	779
20	1000		998	990
22	1120		1100	1118

These data clearly follow the calculations with the flat real potential. To validate further this optical potential, we have proceeded with the calculation of total reaction cross sections and their comparison with phenomenological predictions deduced in Ref. [33]. We have chosen two potentials appearing in Fig. 1. In both of them we refer to the same imaginary part, designated in the figure with the solid red line. For the real part we have chosen the one with the flat line at  $N_R = 0.5$ , taking into account the compatibility of the obtained total reaction cross sections for  ${}^7\text{Be}$  as appear in Table I, under the column flat1. At the lower energy we find some disagreement with the prediction and therefore we proceed with some improvement at the imaginary part. As such we have preferred the suggestion of Ref. [34], and a constant step below  $E/V_{C.b.} = 1$  is adopted—see dot-dashed blue line in Fig. 1. This assumes the possibility of a continuous loss of flux from the elastic channel below threshold, possibly via Coulomb breakup, an issue not unreasonable. The new total reaction cross section results appear now in Table I, under the column with the name flat2, and present a very good consistency with the predictions. Finally results with the same imaginary potential as for flat1 are adopted, and for the real potential the one produced under a dispersive correction, solid red line in the same figure. The results are also included in Table I, under the column disp. The agreement is in principle fair. Taking into account our calculations for both fusion and total reaction cross sections, we conclude that an optical potential with a standard imaginary part, dropping to zero approaching the barrier from higher to lower energies, is necessary but which at below barrier energies develops a constant trend, absorbing continuously flux out of elastic. This is not connected however with a real one which is obtained via a dispersive correction, posing the question of a noncausality for the scattering process of this system or the inadequacy of a mathematical formalism to describe all systems simultaneously. We will come back on this point later on.

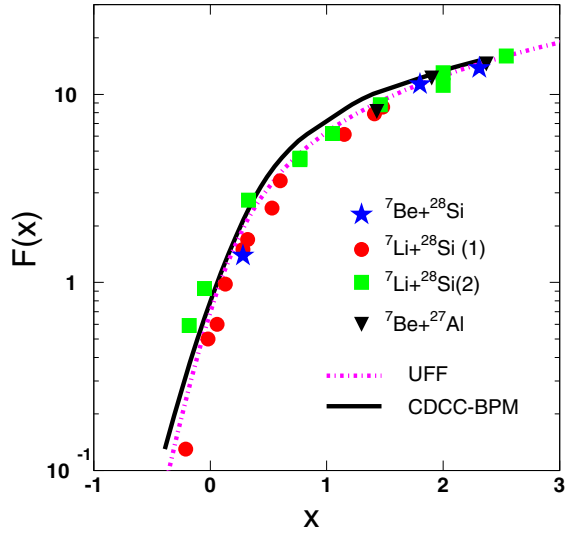


FIG. 4. Excitation fusion function of CDCC-BPM calculations for  ${}^7\text{Be} + {}^{28}\text{Si}$  (see text) are compared with data of  ${}^7\text{Be}$  and  ${}^7\text{Li}$  on the  ${}^{28}\text{Si}$  target [8,27–31] and the UFF curve. It is obvious that coupling to continuum is negligible and of no importance.

### B. CDCC calculations

Our two-body CDCC calculations for elastic scattering are described in Ref. [9] with the  ${}^7\text{Be}$  nucleus to be assumed with a two-body  ${}^4\text{He} + {}^3\text{He}$  cluster structure. Couplings to resonant and nonresonant cluster states corresponding to  ${}^4\text{He} + {}^3\text{He}$  relative orbital angular momenta  $L = 0, 1, 2, 3$ , and  $4 \hbar$  were included. Excitation to the first excited state and ground state reorientation were also taken into account. All the diagonal and coupling potentials were generated from empirical  $\alpha + {}^{28}\text{Si}$  and  ${}^3\text{He} + {}^{28}\text{Si}$  optical model potentials [35,36], by means of the single-folding technique. We should underline here that the coupling potential is the one used in Ref. [14]. To obtain fusion in this formalism we follow the prescription appearing in [37] and applied also in Refs. [23,31] in a BPM framework. In this approach, an effective nuclear potential has to be formed as the sum of the bare potential and the dynamic polarization potential (DPP). The dynamic polarization potential was derived from our CDCC calculations following the prescription of Thompson *et al.* [38]. Our calculation is compared with reduced data [32] (see Eqs. [1] to [2]) in Fig. 4, of  ${}^7\text{Li}$  and  ${}^7\text{Be}$  on  ${}^{28}\text{Si}$  and Wong calculations—UFF curve. Calculations without coupling to continuum were also performed but the difference with the CDCC ones was approximately of the order of  $\approx 4\%$  and are not included in the figure for reasons of clarity. We should note that no coupling to collective states of  ${}^{28}\text{Si}$  are applied either to the no coupling calculations or the CDCC ones. While there is some overestimation of the data the conclusion of this comparison is that coupling to continuum is weak and of no importance for this light target.

## III. THE ${}^7\text{Be} + {}^{208}\text{Pb}$ SYSTEM

### A. The phenomenological description

Previous elastic scattering data for  ${}^7\text{Be} + {}^{208}\text{Pb}$  [7] and  ${}^7\text{Li} + {}^{208}\text{Pb}$  [34] were analyzed into the same microscopic

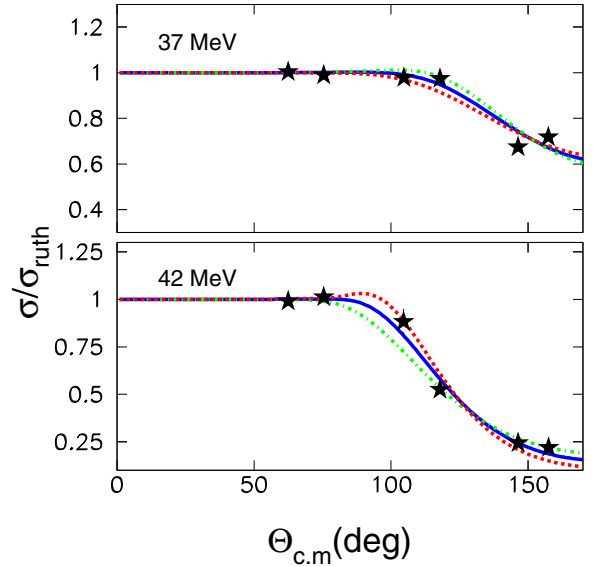


FIG. 5. Previous elastic scattering angular distribution data for  ${}^7\text{Be} + {}^{208}\text{Pb}$ , reported in Ref. [7], were fitted in a BDM3Y1 microscopic framework. The fit is designated with the solid blue line. Other lines were produced in a sensitivity analysis approach, see text. The Coulomb barrier was calculated according to Broglia [22].

BDM3Y1 framework as above for the light target  ${}^{28}\text{Si}$ . Example angular distributions for  ${}^7\text{Be} + {}^{208}\text{Pb}$  are presented in Fig. 5. The best fits were obtained by taking into account the same imaginary potential as for the real part, but with different normalization factors. The density distribution for  ${}^7\text{Be}$ ,  ${}^7\text{Li}$  was also the same as above, while for  ${}^{208}\text{Pb}$  the nuclear matter density was adopted from electron scattering data [16], appropriately corrected to derive it. A sensitivity analysis was performed for determining the uncertainties on the normalization values. The energy dependence of the OM potentials after fits to elastic scattering data for both projectiles  ${}^7\text{Be}$  and  ${}^7\text{Li}$  on a  ${}^{208}\text{Pb}$  target are displayed in Fig. 6. While the data for  ${}^7\text{Be}$  were few, the trend for the potential was more clear taking into account the data for  ${}^7\text{Li}$ . Describing the imaginary potential into the two segment approach [1–3], two trials are shown in Fig. 6, we were able to describe the real part through the dispersion correction [1–3]. Subsequently it was necessary to validate the suggested potential—solid black line in the figure. Two observables were used for fusion and total reaction cross sections. Fusion data do not exist for  ${}^7\text{Be} + {}^{208}\text{Pb}$ , but do exist for other heavy targets, as well as for  ${}^9\text{Be}$  and  ${}^7\text{Li}$  on various heavy targets [39–43]. Taking this opportunity, we have calculated fusion for  ${}^7\text{Be} + {}^{208}\text{Pb}$  in one BPM approach [24,25] and compare with the above experimental data in a reduced form [32]. Our BPM results are included in Fig. 7, and exhibit an excellent agreement with the various data. Additionally a large enhancement versus the UFF curve (Wong approach without couplings) is observed indicating that including explicitly the energy dependence of OMP, we can describe adequately well fusion data at near and sub-barrier energies down to  $0.85V_{c.b.}$ . Further on to validate our suggested potential we present in Table II, total reaction cross sections deduced within this potential, in comparison with previous

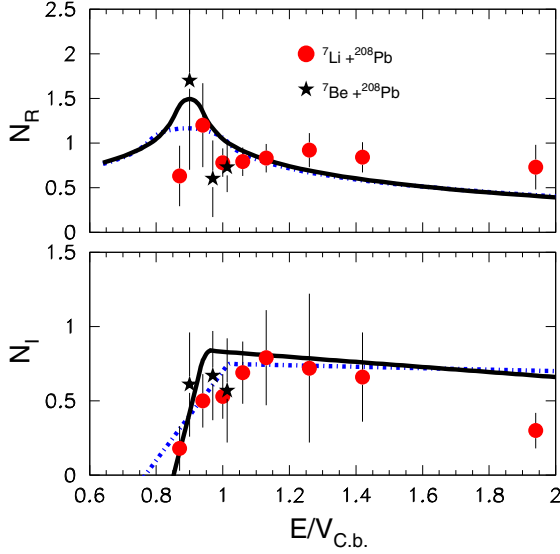


FIG. 6. Energy dependence of the potentials of  ${}^7\text{Be}$  and  ${}^7\text{Li}$  on a  ${}^{208}\text{Pb}$  target. The data are deduced in a BDM3Y1 framework. Two different lines are drawn for describing the imaginary part of the potential and the relevant dispersion correction for the real part is deduced. The Coulomb barrier was calculated according to Broglia [22].

phenomenological predictions [33]. The agreement is adequately good reinforcing our argument that the potential described with the solid black line in Fig. 6, can describe simultaneously elastic scattering, fusion, and total reaction cross sections.

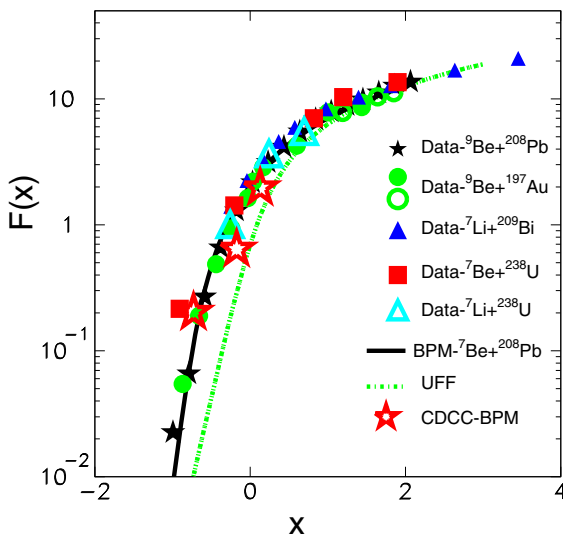


FIG. 7. Excitation fusion function of BPM calculations for  ${}^7\text{Be} + {}^{208}\text{Pb}$  according to the potentials described in Fig. 6 with the solid black line. The results are compared with data of  ${}^9\text{Be}$  and  ${}^7\text{Li}$  on various heavy targets [34,39–43].

TABLE II. Total reaction cross sections, disp, are calculated taking into account the potential, as described by dispersion relations in Fig. 6, solid black line. These are compared with phenomenological predictions [33], designated as pred, exhibiting a very good agreement with them.

$E_{\text{lab}}$ (MeV)	$\sigma$ (mb)	
	disp	pred
37	56	44
40	333	277
42	474	474
46.4	835	859

### B. CDCC calculations

CDCC calculations for the elastic scattering of  ${}^7\text{Be} + {}^{208}\text{Pb}$  are comprehensively discussed in Ref. [7]. Into this formalism, preliminary values for fusion via a BPM approach at three energies were obtained by private communication [44] and compared with data in Fig. 7. These values present an adequate compatibility with the data and the BPM phenomenological calculation. It is apparent that here, contrary to the light target, the coupling to continuum leading to a fusion enhancement is strong. Some space possibly is left for other couplings as to transfer.

### IV. FUSION HINDRANCE

The phenomenon of fusion hindrance has been well established by now for medium and heavy combinations of projectile target [4,5,45]. Initially it was traced through deviations between measured fusion cross sections and coupled channel (CC) calculations at deep sub-barrier energies [46]. Later, for avoiding model calculation dependences, a more accurate determination of the threshold energy for hindrance was suggested. This could be accomplished via excitation functions of astrophysical  $S$  factors and their maximum or/and via the crossing point between the logarithmic derivative of the  $S$  factor and the relevant constant astrophysical  $S$  factor [46,47]. The astrophysical  $S$  factors are given by

$$S(E) = \sigma(E)E \exp(2\pi\eta), \quad (3)$$

where  $\eta$  is the Sommerfeld parameter,

$$\eta = \frac{Z_1 Z_2 e^2}{(\hbar v)} \quad (4)$$

with  $v$  the relative velocity of the colliding ions and  $Z_1, Z_2$  their atomic numbers.

The logarithmic derivative is given by

$$L(E) = d[\ln(\sigma(E)E)]/dE \quad (5)$$

and the constant  $S$  factor as

$$L_{CS} = \frac{\pi\eta}{E}. \quad (6)$$

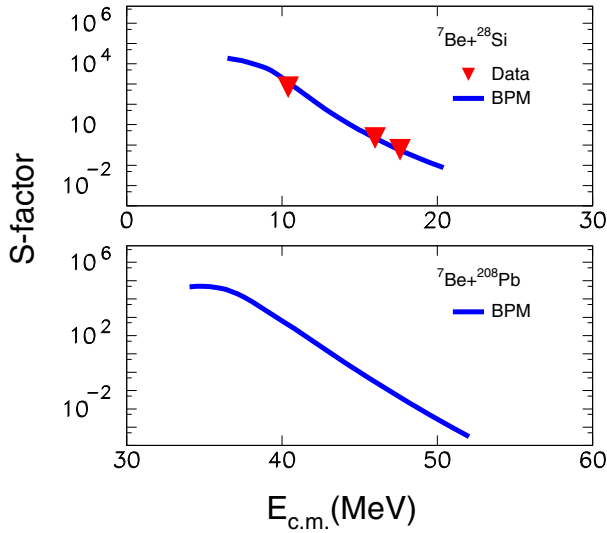


FIG. 8. Excitation functions of astrophysical  $S$  factors as a function of projectile energy for (a)  ${}^7\text{Be} + {}^{28}\text{Si}$  and (b)  ${}^7\text{Be} + {}^{208}\text{Pb}$ . Data are from Ref. [8]. Lines are from present calculations.

Astrophysical factors and logarithmic derivatives are related [47] as

$$\frac{dS}{dE} = S(E) \left[ L(E) - \frac{\pi\eta}{E} \right]. \quad (7)$$

Therefore the astrophysical  $S$  factor presents a maximum at  $L_{CS} = \pi\eta/E$ , the crossing point between the logarithmic derivative and the constant astrophysical  $S$  factor.

In this work the data considered concerned total fusion at near barrier energies for  ${}^7\text{Be} + {}^{28}\text{Si}$  while we have no fusion data for  ${}^7\text{Be} + {}^{208}\text{Pb}$ . However our fusion BPM calculation, performed with the energy dependent potential, deduced from elastic scattering data was found to describe in an excellent way fusion data below barrier for  ${}^7\text{Li} + {}^{28}\text{Si}$ , see Fig. 3, and data of  ${}^7\text{Li}$ ,  ${}^7\text{Be}$ , and  ${}^9\text{Be}$  on various heavy targets as  ${}^{197}\text{Au}$ ,  ${}^{208}\text{Pb}$ , and  ${}^{238}\text{U}$ , see Fig. 7. This give us the justification for seeking the hindrance threshold energy via our BPM calculations. This can validate further the deduced energy dependence of our potential at deep sub-barrier energies. We should note here that this potential was extracted via a double folding procedure and a BDM3Y1 interaction. Such potentials have been suggested for the description of heavier systems towards the determination of fusion hindrance [48]. In this respect, seeking for the energy where hindrance may occur, we present in Fig. 8, the energy evolution of astrophysical  $S$  factors for  ${}^7\text{Be} + {}^{28}\text{Si}$  and  ${}^7\text{Be} + {}^{208}\text{Pb}$ . We see that tentative maxima may occur at  $E_{c.m.} \approx 7$  MeV and 34 MeV for  ${}^{28}\text{Si}$  and  ${}^{208}\text{Pb}$ , respectively. Subsequently in Figs. 9 and 10, we present the fusion logarithmic slopes of several projectiles on light or heavy targets. For this we present total fusion logarithmic derivatives as a function of  $E_{c.m.} - V_{C.b.}$ . The Coulomb barrier here is taken from the Bass prescription [49], to be compatible with fusion hindrance results to be found in the literature. Together with the fusion data we present results for the fusion BPM calculations for  ${}^7\text{Be}$  on  ${}^{28}\text{Si}$  and  ${}^{208}\text{Pb}$  and fits to the

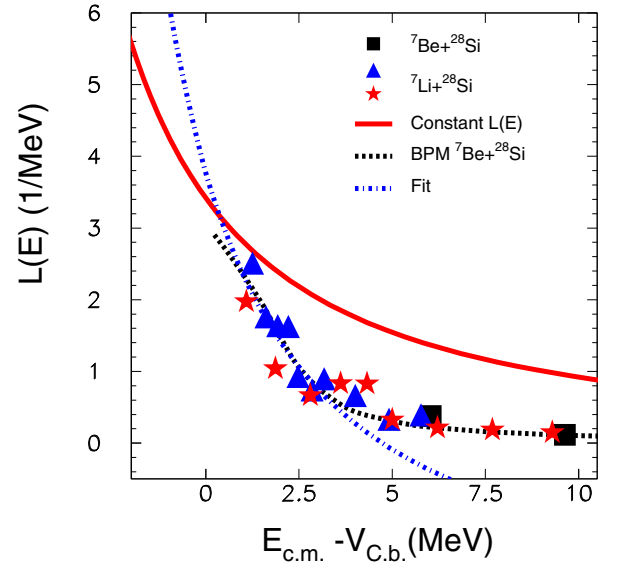


FIG. 9. Calculated logarithmic derivatives as a function of projectile energy minus the barrier for  ${}^7\text{Be} + {}^{28}\text{Si}$ . For that we take into account total fusion cross sections of our BPM approach with the real part of the potential, as extracted from elastic scattering fits—see potential in Fig. 1, designated with the solid cyan flat line. The constant  $S$  factor is also calculated and it is designated with the solid red line. The dot-dashed blue line an extrapolation of fitted data according to Eq. (8) is also shown. Calculations are compared with data for  ${}^7\text{Be} + {}^{28}\text{Si}$ , designated with the black boxes from Ref. [8] and  ${}^7\text{Li} + {}^{28}\text{Si}$  designated with blue triangles from Ref. [30] and red stars from Refs. [28,29]. Barriers were calculated according to the Bass prescription [49], as 7.17 and 5.07 MeV for the two systems, respectively.

lower energy data, according to Ref. [4]:

$$L(E) = A_0 + \frac{B_0}{E^{3/2}}. \quad (8)$$

Experimental crossing points,  $E_s^e$ , between extrapolated logarithmic derivatives,  $L$ , fitted to all data appearing in Figs. 9 and 10 with Eq. (8), and the constant  $S$  factor,  $L_{CS}$ , as well as “theoretical” crossing points where they exist,  $E_s^t$  via our BPM results transformed to logarithmic derivatives, appear in Table III. Experimental crossings appear at 7.6 MeV for the light target ( ${}^7\text{Be} + {}^{28}\text{Si}$ ) and at 33.5 MeV for the heavy target ( ${}^7\text{Be} + {}^{208}\text{Pb}$ ). Similar values are obtained for  ${}^7\text{Li} + {}^{28}\text{Si}$  and  ${}^7\text{Li}$  and  ${}^9\text{Be}$  on various heavy targets. These values are compared with other existing values of well bound projectiles. The obtained ratios of the crossing energy  $E_s^e$  versus the Coulomb barrier according to the Bass model, are also included. An inspection of Figs. 9 and 10 and Table III underlines a strong differentiation between the appearance of fusion hindrance via logarithmic derivatives of the weakly bound projectiles with a light and a heavy target. For the light target, the logarithmic slope of the  $S$  factor for the BPM representation of fusion cross sections does not cross the constant  $S$  factor,  $L_{CS}$ , but it proceeds in a parallel path to it. The extrapolation of the data via the fit with Eq. (8) does. We should mention however here that if we include in the fit data points at higher energies up to  $E_{c.m.} - V_{C.b.} = 4.5$

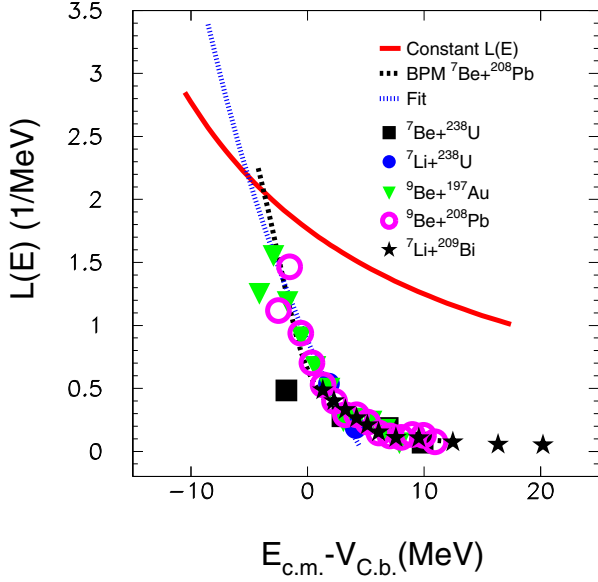


FIG. 10. Calculated logarithmic derivatives as a function of projectile energy minus the barrier, according to our BPM approach with the potential appearing in Fig. 6, with the black solid line. The constant  $S$  factor is also shown as well as the extrapolation of the data fits via Eq. (8). Data are from Refs. [34,39–43] for  ${}^7\text{Be} + {}^{238}\text{U}$ ,  ${}^7\text{Li} + {}^{208}\text{Pb}$ ,  ${}^7\text{Li} + {}^{198}\text{Pt}$ ,  ${}^7\text{Li} + {}^{238}\text{U}$ ,  ${}^9\text{Be} + {}^{197}\text{Au}$ ,  ${}^9\text{Be} + {}^{208}\text{Pb}$ ,  ${}^9\text{Be} + {}^{238}\text{U}$ , with barriers according to the Bass prescription as 42.56, 27.74, 26.5, 30.67, 36.37, 37.42, 41.41, respectively.

then the extrapolated line does not cross either the constant  $S$  curve but proceeds in parallel to it, like our BPM calculation. This is contrary to the behavior of the heavy target, where a clear cross point is evident for both, data extrapolation and BPM calculation, in good compatibility between them (see

TABLE III. Threshold hindrance energies, determined in this work for weakly bound projectiles on various targets through previous total fusion experimental data,  $E_s^e$ , and through present calculations,  $E_s^l$ , are compared with results of well bound systems. Reference energies are also included  $E_s^r$ ;  $E_s^r = 0.356\zeta^{2/3}$  with  $\zeta = Z_1Z_2\sqrt{(M_1M_2/(M_1 + M_2))}$  [4]. All energies are given in MeV, including the  $Q$  value of the fusion reaction. Ratios of threshold energies versus the Coulomb barrier are formed taking into account the Bass formalism [49].

System	$Q$	$E_s^r$	$E_s^e$	$E_s^l$	$E_s^e/V_B$	$E_s^l/V_B$	Ref.
${}^7\text{Be} + {}^{208}\text{Pb}$	-4.81	32	33.5	34.75	0.87	0.9	present
${}^7\text{Be} + {}^{238}\text{U}$	2.73	34.62	37.53	38.78	0.88	0.91	present
${}^9\text{Be} + {}^{208}\text{Pb}$	-14.06	34.71	32.45	33.7	0.87	0.9	present
${}^9\text{Be} + {}^{197}\text{Au}$	0.235	33.83	31.34	32.29	0.86	0.9	present
${}^7\text{Li} + {}^{209}\text{Bi}$	-3.60	26.65	23.07	24.32	0.82	0.87	present
${}^{11}\text{B} + {}^{197}\text{Au}$	-5	41.8	40		0.87		[54]
${}^{12}\text{C} + {}^{198}\text{Pt}$	-13.96	48.2	50		0.87		[55]
${}^{16}\text{O} + {}^{208}\text{Pb}$	-46.48	66	68		0.88		[56]
${}^7\text{Be} + {}^{28}\text{Si}$	17.32	9.25	7.6		1.06		present
${}^7\text{Li} + {}^{28}\text{Si}$	22.43	7.64	5.51		1.09		present
${}^{12}\text{C} + {}^{30}\text{Si}$	14.11	14	10.5		0.97		[57]

Table III). A common point between the systems with the light and heavy target is that the logarithmic derivative as a function of energy, as we go from higher to lower energies, presents a continuous increasing trend without to present a saturation. Such behavior is similar to the one with medium or heavy well bound systems as, e.g., the symmetric ones  ${}^{58}\text{Ni} + {}^{54}\text{Fe}$  and  ${}^{58}\text{Ni}$  and  ${}^{58}\text{Ni}$  [50] or, e.g., asymmetric  ${}^{60}\text{Ni} + {}^{89}\text{Y}$  [47]. For other systems either asymmetric  ${}^{11}\text{B} + {}^{197}\text{Au}$  [54] and  ${}^{36}\text{S} + {}^{48}\text{Ca}$  [51], light symmetric  ${}^{28}\text{Si} + {}^{28}\text{Si}$  [52], and medium mass  ${}^{40}\text{Ca} + {}^{48}\text{Ca}$ ,  ${}^{40}\text{Ca} + {}^{40}\text{Ca}$  [53], the increasing trend of the logarithmic derivative presents a saturation-plateau range between  $E/V_{C.b.} \approx 0.98$  to  $0.92$  and then continues to increase crossing the constant  $S$  factor at lower energies between  $E/V_{C.b.} \approx 0.83$  to  $0.89$ . And while we cannot find a common point to systematize the above, apparently due to a mixing of different reaction dynamics, we could claim that for weakly bound nuclei on heavy targets, the threshold energies for hindrance are close to ones for well bound systems. For light targets though as the reaction mechanism is very different as was outlined from the energy dependence of the OM potential and the lack of fusion enhancement, either we have no evidence of a fusion hindrance or possibly it starts from the barrier and below. The last is in accordance with the similar system  ${}^{12}\text{C} + {}^{30}\text{Si}$ , reported in Ref. [57]. In that case while the CC calculation develops in a parallel path to the constant  $S$  factor, the extrapolation of the data crosses it at  $10.5$  MeV (Table III) that is at  $E/V_{C.b.} = 0.97$ . In our case our BPM calculation proceeds also in a parallel basis to the  $L_{CS}$ , while the data extrapolation crosses it at  $E/V_{C.b.} \approx 1.1$ . This is in some agreement with the findings of Fowler *et al.* [58] for  ${}^{12}\text{C} + {}^{16}\text{O}$  where the extrapolation recipe leads to a logarithmic slope

$$L = L_{CS} - \alpha, \quad (9)$$

where  $\alpha = 0.64 \text{ MeV}^{-1}$  and therefore the logarithmic derivative of the astrophysical  $S$  factor will never cross the  $L_{CS}$  curve.

We should underline here that our study and our conclusions for fusion hindrance for weakly bound projectiles refers to total fusion data and calculations or/and extrapolated fits to data. They are all mean values extracted from the consideration of various projectiles and targets. Previous results for  ${}^6\text{Li}$  and  ${}^7\text{Li}$  on heavy targets refer to complete fusion data [54,59] and were found to support possible fusion hindrance below  $E/V_{C.b.} = 0.65$  to  $0.71$ , respectively.

## V. DISCUSSION—CONCLUSIONS

We have studied the reaction dynamics of  ${}^7\text{Be} + {}^{28}\text{Si}$  and  ${}^7\text{Be} + {}^{208}\text{Pb}$  at near and sub-barrier energies. The energy dependence of the optical potential was probed in a coherent analysis of previous elastic scattering and fusion data for  ${}^7\text{Be} + {}^{28}\text{Si}$  and  ${}^7\text{Li}$  and  ${}^9\text{Be}$  on various light and heavy targets  ${}^{28}\text{Si}$ ,  ${}^{208}\text{Pb}$ ,  ${}^{238}\text{U}$ . Our microscopic phenomenological approach was based on double folding potentials of the BDM3Y1 interaction and appropriate matter densities. BPM calculations were made taking into account the energy dependence of the optical potential extracted from elastic scattering data for  ${}^7\text{Be}$  on  ${}^{28}\text{Si}$  and  ${}^{208}\text{Pb}$  and dispersion calculations where it applied. The validity of these results were confronted with the excellent agreement of total fusion data of  ${}^7,9\text{Be}$  and

${}^7\text{Li}$  on various light and heavy targets and by the consideration of total reaction cross sections, determined before via systematics [33]. This gave us the justification for seeking the phenomenon of fusion hindrance of the weakly bound radioactive nucleus,  ${}^7\text{Be}$ , as well of the weakly bound but stable nuclei  ${}^7\text{Li}$  and  ${}^9\text{Be}$  on light and heavy targets. Throughout this work we noticed a clear distinction between the two systems under investigation:  ${}^7\text{Be} + {}^{28}\text{Si}$  and  ${}^7\text{Be} + {}^{208}\text{Pb}$ . The same behavior was closely followed by  ${}^7\text{Li}$  on the same targets. This refers to the energy dependence of the optical potential, as well as to the consequences of this on fusion

In summary

- (1) The behavior of  ${}^7\text{Be}$  and  ${}^7\text{Li}$  reacting at light and heavy targets at near and sub-barrier energies in respect with the OM potential is similar.
- (2) The energy dependence of the OM potential of  ${}^7\text{Be}$  and  ${}^7\text{Li}$  on light targets is clearly diverting from the one with a heavy target. For light targets the energy dependence of the real part of the potential is constant (the normalization factor of the real part of the potential can be represented by a flat line), at least between the energy range under investigation 0.8 to 1.2  $E/V_{C,b}$ . For the imaginary part we have the usual drop around barrier, but which continuous as a step going to sub-barrier energies, absorbing continually flux from elastic. On the other hand for heavy targets we observe the standard potential threshold anomaly obeying the dispersion relations. Is that a sign that the causality principle is not valid for light targets and the scattering and reaction processes involved? Or it is simply a lack of an appropriate mathematical representation of the potential for both targets?
- (3) Fusion for the mirror nuclei  ${}^7\text{Be}$  and  ${}^7\text{Li}$  on light targets are compatible with simple Wong predictions at near and sub-barrier energies (0.8 to 1.2  $V_{C,b}$ ) and BPM calculations taking into account a flat real OM potential. No enhancement is observed. This could be understood for light systems, where we expect the absence of couplings to internal degrees of freedom. These are connected with the product of atomic numbers of the colliding nuclei  $Z_1 Z_2$  [4,60]. Further on our CDCC calculations support very small breakup cross sections, of the order of  $\mu\text{b}$ , and negligible couplings to continuum not playing a crucial role either.

- (4) On the contrary, fusion for the mirror nuclei  ${}^7\text{Be}$  and  ${}^7\text{Li}$  on heavy targets is substantially enhanced versus Wong predictions, and can be described by BPM calculations as long as the OM potential energy dependence is taken into account. The last being compatible with a description via dispersion relations. The fusion enhancement according to CDCC calculations can be interpreted to be mainly due to continuum excitations. Here, we have a strong coupling related to a moderate breakup cross sections ( $\approx 10\%$  of total reaction—see Ref. [7]).
- (5) Excitation functions of logarithmic derivatives, extracted from BPM fusion calculations as the above, can be probably used for determining threshold fusion hindrance energies, as cross points between them and the constant astrophysical  $S$  factors. In the present work it became evident that for all weakly bound projectiles  ${}^7\text{Be}$ ,  ${}^9\text{Be}$ , and  ${}^7\text{Li}$  on heavy targets a potentially threshold fusion hindrance will appear at  $E_s^w/V_{C,b} \approx 0.87$  in very good compatibility with threshold energies for well bound projectiles as  ${}^{11}\text{B}$ ,  ${}^{12}\text{C}$ , and  ${}^{16}\text{O}$  on heavy targets. An experimental indication for fusion hindrance for weakly bound nuclei on heavy targets at deep sub-barrier energies is given by the results in Refs. [33,61], reporting on direct reactions dominance at deep sub-barrier energies. In this work experimental breakup cross sections exhausted all the reaction probability at energies  $E/V_{C,b} \approx 0.7$ .
- (6) For light targets the situation is very different. The logarithmic derivative extracted from our BPM calculations develops from higher to lower energies in a parallel path to the constant astrophysical  $S$  factor at deep sub-barrier energies. Extrapolation of the data, depending on the data which are included in the fit, predict either no crossing as the BPM calculation or a crossing around  $E_s^e/V_{C,b} \approx 1.1$ . All the above imply that for weakly bound projectiles on light targets fusion develops smoothly without neither a cross section enhancement close to the barrier nor an apparent fusion hindrance.

## ACKNOWLEDGMENTS

We warmly acknowledge Prof. Krzysztof Rusek and Dr. Jesus Casal for enlightening discussions.

- 
- [1] G. R. Satchler, *Phys. Rep.* **199**, 147 (1991).
  - [2] M. A. Nagarajan, C. C. Mahaux, and G. R. Satchler, *Phys. Rev. Lett.* **54**, 1136 (1985).
  - [3] M. A. Nagarajan and G. R. Satchler, *Phys. Lett. B* **173**, 29 (1986).
  - [4] C. L. Jiang, B. B. Back, K. E. Rehm, K. Hagino, G. Montagnoli, and A. M. Stefanini, *Eur. Phys. J. A* **57**, 235 (2021).
  - [5] B. B. Back, H. Esbensen, C. L. Jiang, and K. E. Rehm, *Rev. Mod. Phys.* **86**, 317 (2014).
  - [6] N. Keeley, K. W. Kemper, and K. Rusek, *Phys. Rev. C* **66**, 044605 (2002).
  - [7] M. Mazzocco *et al.*, *Phys. Rev. C* **100**, 024602 (2019).
  - [8] O. Sgouros *et al.*, *Phys. Rev. C* **94**, 044623 (2016).
  - [9] O. Sgouros *et al.*, *Phys. Rev. C* **95**, 054609 (2017).
  - [10] R. H. Cyburt, B. D. Fields, K. A. Olive, and T.-H. Yeh, *Rev. Mod. Phys.* **88**, 015004 (2016).
  - [11] P. E. Koehler *et al.*, *Phys. Rev. C* **37**, 917 (1988).
  - [12] M. Barbagallo *et al.*, *Phys. Rev. Lett.* **117**, 152701 (2016).
  - [13] L. Lamia *et al.*, *Astrophys. J.* **850**, 175 (2017).
  - [14] E. M. Tursunov, S. A. Turakulov, and A. S. Kadyrov, *Nucl. Phys. A* **1006**, 122108 (2021).
  - [15] D. T. Khoa and W. von Oertzen, *Phys. Lett. B* **342**, 6 (1995).

- [16] A. Bhagwat, Y. K. Gambhir, and S. H. Patil, *Eur. Phys. J. A* **8**, 511 (2000).
- [17] L. Trache, A. Azhari, H. L. Clark, C. A. Gagliardi, Y.-W. Lui, A. M. Mukhamedzhanov, R. E. Tribble, and F. Carstoiu, *Phys. Rev. C* **61**, 024612 (2000).
- [18] A. Pakou, N. Alamanos, G. Doukelis, A. Gillibert, G. Kalyva, M. Kokkoris, S. Kossionides, A. Lagoyannis, A. Musumarra, C. Papachristodoulou, N. Patronis, G. Perdikakis, D. Pierroutsakou, E. C. Pollacco, and K. Rusek, *Phys. Rev. C* **69**, 054602 (2004).
- [19] N. Keeley, N. Alamanos, K. W. Kemper, and K. Rusek, *Prog. Part. Nucl. Phys.* **63**, 396 (2009).
- [20] K. Zerva *et al.*, *Eur. Phys. J. A* **48**, 102 (2012).
- [21] A. Pakou, V. Soukeras, F. Cappuzzello, L. Acosta, C. Agodi, X. Aslanoglou, S. Calabrese, D. Carbone, M. Cavallaro, A. Foti, N. Keeley, G. Marquinez-Duran, I. Martel, M. Mazzocco, C. Parascandolo, D. Pierroutsakou, K. Rusek, O. Sgouros, E. Strano, and V. A. B. Zagatto, *Phys. Rev. C* **94**, 014604 (2016).
- [22] R. A. Broglia and A. Winther, *Heavy Ion Reactions*, Vol. I: Elastic and Inelastic Reactions (The Benjamin/Cummings Publishing Company, Inc, San Francisco, 1981).
- [23] K. Palli, J. Casal, and A. Pakou, *Phys. Rev. C* **105**, 064609 (2022).
- [24] M. J. Rhoades-Brown and P. Braun-Munzinger, *Phys. Lett. B* **136**, 19 (1984).
- [25] N. Alamanos, *Eur. Phys. J. A* **56**, 212 (2020).
- [26] J. Raynal, *Phys. Rev. C* **23**, 2571 (1981).
- [27] K. Kalita, S. Verma, R. Singh, J. J. Das, A. Jhingan, N. Madhavan, S. Nath, T. Varughese, P. Sugathan, V. V. Parkar, K. Mahata, K. Ramachandran, A. Shrivastava, A. Chatterjee, S. Kailas, S. Barua, P. Basu, H. Majumdar, M. Sinha, R. Bhattacharya, and A. K. Sinha, *Phys. Rev. C* **73**, 024609 (2006).
- [28] M. Sinha, H. Majumdar, R. Bhattacharya, P. Basu, S. Roy, M. Biswas, R. Palit, I. Mazumdar, P. K. Joshi, H. C. Jain, and S. Kailas, *Phys. Rev. C* **76**, 027603 (2007).
- [29] M. Sinha, H. Majumdar, P. Basu, S. Roy, R. Bhattacharya, M. Biswas, M. K. Pradhan, and S. Kailas, *Phys. Rev. C* **78**, 027601 (2008).
- [30] A. Pakou, K. Rusek, N. Alamanos, X. Aslanoglou, M. Kokkoris, A. Lagoyannis, T. J. Mertzimekis, A. Musumarra, N. G. Nicolis, D. Pierroutsakou, and D. Roubos, *Eur. Phys. J. A* **39**, 187 (2009).
- [31] A. Pakou, O. Sgouros, V. Soukeras, J. Casal, and K. Rusek, *Eur. Phys. J. A* **58**, 8 (2022).
- [32] L. F. Canto, P. R. S. Gomes, J. Lubian, L. C. Chamon, and E. Crema, *J. Phys. G* **36**, 015109 (2009).
- [33] A. Pakou *et al.*, *Eur. Phys. J. A* **51**, 55 (2015).
- [34] N. Keeley, N. M. Clarke, B. R. Fulton, G. Tungate, P. V. Drumm, M. A. Nagarajan, and J. S. Lilley, *Nucl. Phys. A* **571**, 326 (1994).
- [35] W. Whur, A. Hofmann, and G. Philipp, *Z. Phys.* **269**, 365 (1974).
- [36] B. H. Wildenthal and P. W. M. Glaudemans, *Nucl. Phys. A* **92**, 353 (1967).
- [37] K. Rusek, N. Alamanos, N. Keeley, V. Lapoux, and A. Pakou, *Phys. Rev. C* **70**, 014603 (2004).
- [38] I. J. Thomson, M. A. Nagarajan, J. S. Lilley, and M. J. Smithson, *Nucl. Phys. A* **505**, 84 (1989).
- [39] R. Raabe, C. Angulo, J. L. Charvet, C. Jouanne, L. Nalpas, P. Figuera, D. Pierroutsakou, M. Romoli, and J. L. Sida, *Phys. Rev. C* **74**, 044606 (2006).
- [40] M. Dasgupta *et al.*, *Phys. Rev. C* **70**, 024606 (2004).
- [41] F. Gollan *et al.*, *Phys. Rev. C* **104**, 024609 (2021).
- [42] M. Kaushik, S. K. Pandit, V. V. Parkar, G. Gupta, S. Thakur, V. Nanal, H. Krishnamoorthy, A. Shrivastava, C. S. Palshetkar, K. Mahata, K. Ramachandran, S. Pal, R. G. Pillay, and P. P. Singh, *Phys. Rev. C* **104**, 024615 (2021).
- [43] G. S. Li *et al.*, *Phys. Rev. C* **100**, 054601 (2019).
- [44] N. Keeley (private communication).
- [45] C. L. Jiang, H. Esbensen, K. E. Rehm, B. B. Back, R. V. F. Janssens, J. A. Caggiano, P. Collon, J. Greene, A. M. Heinz, D. J. Henderson, I. Nishinaka, T. O. Pennington, and D. Seweryniak, *Phys. Rev. Lett.* **89**, 052701 (2002).
- [46] T. Ichikawa, *Phys. Rev. C* **92**, 064604 (2015).
- [47] C. L. Jiang, H. Esbensen, B. B. Back, R. V. F. Janssens, and K. E. Rehm, *Phys. Rev. C* **69**, 014604 (2004).
- [48] S. Misicu and H. Esbensen, *Phys. Rev. C* **75**, 034606 (2007).
- [49] R. Bass, *Nucl. Phys. A* **231**, 45 (1974).
- [50] A. M. Stefanini, G. Montagnoli, L. Corradi, S. Courtin, E. Fioretto, A. Goasduff, F. Haas, P. Mason, R. Silvestri, P. P. Singh, F. Scarlassara, and S. Szilner, *Phys. Rev. C* **82**, 014614 (2010).
- [51] G. Montagnoli, A. M. Stefanini, H. Esbensen, C. L. Jiang, L. Corradi, S. Courtin, E. Fioretto, A. Goasduff, J. Grebosz, F. Haas, M. Mazzocco, C. Michelagnoli, T. Mijatovic, D. Montanari, C. Parascandolo, K. E. Rehm, F. Scarlassara, S. Szilner, X. D. Tang, and C. A. Ur, *Phys. Rev. C* **87**, 014611 (2013).
- [52] G. Montagnoli, A. M. Stefanini, H. Esbensen, C. L. Jiang, L. Corradi, S. Courtin, E. Fioretto, J. Grebosz, F. Haas, H. M. Jia, M. Mazzocco, C. Michelagnoli, T. Mijatovic, D. Montanari, C. Parascandolo, F. Scarlassara, E. Strano, S. Szilner, and D. Torresi, *Phys. Rev. C* **90**, 044608 (2014).
- [53] G. Montagnoli, A. M. Stefanini, C. L. Jiang, H. Esbensen, L. Corradi, S. Courtin, E. Fioretto, A. Goasduff, F. Haas, A. F. Kifle, C. Michelagnoli, D. Montanari, T. Mijatovic, K. E. Rehm, R. Silvestri, P. P. Singh, F. Scarlassara, S. Szilner, X. D. Tang, and C. A. Ur, *Phys. Rev. C* **85**, 024607 (2012).
- [54] A. Shrivastava, K. Mahata, V. Nanal, S. K. Pandit, V. V. Parkar, P. C. Rout, N. Dokania, K. Ramachandran, A. Kumar, A. Chatterjee, and S. Kailas, *Phys. Rev. C* **96**, 034620 (2017).
- [55] A. Shrivastava, K. Mahata, S. K. Pandit, V. Nanal, T. Ichikawa, K. Hagino, A. Navin, C. S. Palshetkar, V. V. Parkar, K. Ramachandran, P. C. Rout, A. Kumar, A. Chatterjee, and S. Kailas, *Phys. Lett. B* **755**, 332 (2016).
- [56] M. Dasgupta, D. J. Hinde, A. Diaz-Torres, B. Bouriquet, C. I. Low, G. J. Milburn, and J. O. Newton, *Phys. Rev. Lett.* **99**, 192701 (2007).
- [57] G. Montagnoli *et al.*, *Phys. Rev. C* **97**, 024610 (2018).
- [58] W. A. Fowler, G. R. Caughlan, and B. A. Zimmerman, *Annu. Rev. Astron. Astrophys.* **13**, 69 (1975).
- [59] A. Shrivastava, A. Navin, A. Lemasson, K. Ramachandran, V. Nanal, M. Rejmund, K. Hagino, T. Ichikawa, S. Bhattacharyya, A. Chatterjee, S. Kailas, K. Mahata, V. V. Parkar, R. G. Pillay, and P. C. Rout, *Phys. Rev. Lett.* **103**, 232702 (2009).
- [60] K. Hagino and N. Takigawa, *Prog. Theor. Phys.* **128**, 1061 (2012).
- [61] A. Pakou *et al.*, *Phys. Rev. C* **102**, 031601(R) (2000).